



Full length article

Lipopeptisomes: Anticancer peptide-assembled particles for fusolytic oncotherapy



Matthew R. Aronson^{a,1}, Andrew W. Simonson^{a,1}, Lindsey M. Orchard^b, Manuel Llinás^{b,c,d}, Scott H. Medina^{a,*}

^a Department of Biomedical Engineering, The Pennsylvania State University, University Park, PA 16802, USA

^b Department of Biochemistry and Molecular Biology, The Pennsylvania State University, University Park, PA 16802, USA

^c Department of Chemistry, The Pennsylvania State University, University Park, PA 16802, USA

^d Huck Center for Malaria Research, The Pennsylvania State University, University Park, PA 16802, USA

ARTICLE INFO

Article history:

Received 29 May 2018

Received in revised form 28 August 2018

Accepted 17 September 2018

Available online 19 September 2018

Keywords:

Peptide
Self-assembly
Drug delivery
Nanomedicine

ABSTRACT

Anticancer peptides (ACPs) are cationic amphiphiles that preferentially kill cancer cells through folding-dependent membrane disruption. Although ACPs represent attractive therapeutic candidates, particularly against drug-resistant cancers, their successful translation into clinical practice has gone unrealized due to their poor bioavailability, serum instability and, most importantly, severe hemolytic toxicity. Here, we exploit the membrane-specific interactions of ACPs to prepare a new class of peptide-lipid particle, we term a lipopeptisome (LP). This design sequesters loaded ACPs within a lipid lamellar corona to avoid contact with red blood cells and healthy tissues, while affording potent lytic destruction of cancer cells following LP-membrane fusion. Biophysical studies show ACPs rapidly fold at, and integrate into, liposomal membranes to form stable LPs with high loading efficiencies (>80%). Rational design of the particles to possess lipid combinations mimicking that of the aberrant cancer cell outer leaflet allows LPs to rapidly fuse with tumor cell membranes and afford localized assembly of loaded ACPs within the bilayer. This leads to preferential fusolytic killing of cancer cells with minimal collateral toxicity towards non-cancerous cells and erythrocytes, thereby imparting clinically relevant therapeutic indices to otherwise toxic ACPs. Thus, integration of ACPs into self-assembled LPs represents a new delivery strategy to improve the therapeutic utility of oncolytic agents, and suggests this technology may be added to targeted combinatorial approaches in precision medicine.

Statement of Significance

Despite their significant clinical potential, the therapeutic utility of many ACPs has been limited by their collateral hemolysis during administration. Leveraging the membrane-specific interactions of ACPs, here we prepare self-assembled peptide-lipid nanoparticles, or 'lipopeptisomes' (LPs), capable of preferentially fusing with and lysing cancer cell membranes. Key to this fusolytic action is the construction of LPs from lipids simulating the cancer cell outer leaflet. This design recruits the oncolytic peptide payload into the carrier lamella and allows for selective destruction of cancer cells without disrupting healthy cells. Consequently, LPs impart clinically relevant therapeutic indexes to previously toxic ACPs, and thus open new opportunities to improve the clinical translation of oncolytics challenged by narrow therapeutic windows.

© 2018 Acta Materialia Inc. Published by Elsevier Ltd. All rights reserved.

1. Introduction

Anticancer peptides (ACPs) are a class of cationic amphiphiles that preferentially bind to and disrupt cancer cell membranes through folding dependent mechanisms [1,2]. Sharing similar structural and physicochemical properties to antimicrobial peptides, many ACPs were in fact originally identified as antibacterials

* Corresponding author.

E-mail address: shm126@psu.edu (S.H. Medina).

¹ Co-first author.

before discovery of their preferential anticancer activity [3]. The selectivity of ACPs to lyse tumor cells is largely driven by the increased electronegative potential of the cancer cell surface, which serves to distinguish malignant phenotypes from their more neutral, non-cancerous counterparts. This high net-negative charge results from increased presentation of the anionic lipid phosphatidylserine in the outer leaflet of cancer cell membranes [4–6], as well as abnormal sialylation of cell surface glycoproteins [7–9]. Electrostatic association of cationic ACPs with the electronegative cancer cell surface drives the folding of these sequences into α -helical or β -rich bioactive conformations [3,10]. Once bound, aqueous exposure of the peptide's hydrophobic face promotes its insertion into the lipid bilayer, where subsequent peptide assembly leads to the formation of lytic pores that disrupt membrane integrity and cause cancer cell death.

Importantly, due to their membrane-specific mechanisms of action, many oncolytic peptides show equal potency towards both drug-sensitive and multidrug resistant cancer cell lines [1,2,11–13]. Further, the ability of ACPs to disrupt cellular membranes in a rapid and non-stereospecific fashion has encouraged the perception that *in vivo* resistance towards these agents may be difficult to acquire [3]. In fact, we have previously shown that although cancer cells can develop diminished sensitivity towards a model oncolytic peptide during *in vitro* culture, the loss of ACP potency is marginal compared to conventional chemotherapeutic resistance [14]. These cells also display a surface glycosylation pattern that suggests they may have lost their invasive phenotype, indicating oncolytic peptides may serve as potential anti-metastatic agents. Together, these unique therapeutic properties of ACPs have led to growing interest in developing combinatorial treatments using oncolytic peptides and small molecule inhibitors as potentially successful strategies in the clinic to limit resistance.

Yet, despite their significant therapeutic potential, the clinical translation of ACPs has been limited by their rapid systemic clearance and poor distribution to tumor tissue [15]. This necessitates large doses of ACPs to be administered *in vivo*, often at or above tolerated concentrations, to achieve antitumor responses [12,15,16]. The resulting hemolysis and destruction of healthy cells at these high concentrations ultimately leads to severe dose-limiting toxicities. This off-target activity of ACPs is largely due to the small, but still significant, presence of negatively charged lipids, such as phosphatidylethanolamine, on the outer membrane of healthy mammalian tissues and red blood cells [17–19]. Although not as abundant as on the surfaces of cancer cells [4–6], this modest anionic charge is sufficient to potentiate the binding of ACPs and cause damage to non-cancerous cell membranes at high peptide concentrations. Thus, delivery systems that can localize ACPs to tumor tissue and preferentially integrate the lytic cargo into cancer cell membranes, while evading off-target toxicity towards red blood cells and healthy tissues, represent an attractive strategy to improve the clinical utility of these potentially potent and efficacious anticancer drug candidates.

In this work, we leverage the membrane-specific interactions of ACPs to prepare a new class of peptide-loaded lipid particle, which we term a lipopeptisome (LP) (Fig. 1). This design pre-folds loaded ACPs into their bioactive lytic state, while sequestering the peptide cargo from proteases and red blood cells in the systemic circulation. Fusion of LPs with cancer cell membranes leads to direct assimilation of loaded ACPs into the lipid bilayer, where subsequent peptide self-assembly forms lytic pores. This strategy allows LPs to elicit preferential fusolytic killing of cancer cells while being remarkably biocompatible towards healthy cells and erythrocytes; thus affording clinically viable therapeutic indices to otherwise highly toxic ACPs. Hence, LPs may serve as a simple, effective delivery platform to improve the efficacy and safety profile of oncolytic molecules challenged by poor stability and off-target side effects.

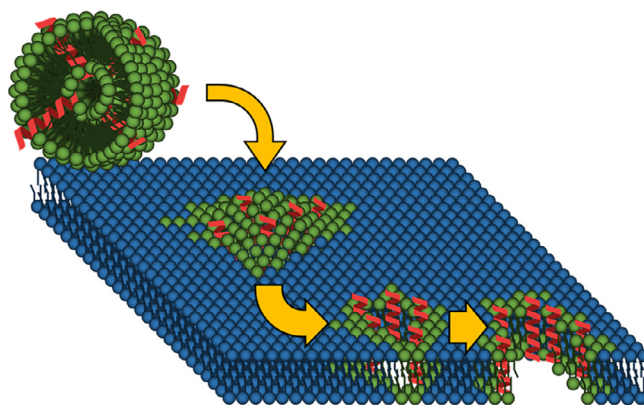


Fig. 1. Schematic illustration of LP composition and proposed fusolytic anticancer mechanism. Particles are formed via integration of ACPs (red) within a liposomal carrier (green) which possesses a similar lipid composition to that of the cancer cell membrane (shown in blue for clarity). The resulting fusion of LPs with cancer cell membranes leads to direct assimilation of loaded ACPs within the lipid bilayer. Subsequent peptide self-assembly forms lytic pores that leads to preferential tumor cell lysis.

2. Materials and methods

2.1. Materials

1,2-Ethanedithiol and diethyl ether were purchased from Acros Organics. 1,3 Bis[tris(hydroxymethyl)methylamino]propane (BTP), piperidine, dimethyl sulfoxide spectrophotometer grade (DMSO), and thioanisole were purchased from Alfa Aesar. Normal Human Primary Umbilical Vein Endothelial Cells (HUVECs), Rh VEGF, rg EGF, rg FGF basic, rg IGF-1, L-glutamine, heparin sulfate, hydrocortisone hemisuccinate, fetal bovine serum (FBS), and ascorbic acid were purchased from ATCC. 1-Palmitoyl-2-oleoyl-sn-glycero-3-phosphocholine (POPC), 1-palmitoyl-2-oleoyl-sn-glycero-3-phospho-L-serine (POPS), 1,2-dioleoyl-sn-glycero-3-phosphoethanolamine (DOPE), and 1,2-dioleoyl-sn-glycero-3-phosphoethanolamine-N-(lissamine rhodamine B sulfonyl) (PE_{rhodamine}) were purchased from Avanti Polar Lipids. Sodium fluoride and sodium hydroxide were purchased from BDH. Fmoc-protected amino acids, oxyma, and Rink Amide ProTide Resin were purchased from CEM. Paraformaldehyde was purchased from Chem Cruz. 5(6)-Carboxyfluorescein, 3-(4,5-dimethyl-2-thiazolyl)-2,5-diphenyl-2H-tetrazolium bromide (MTT), fmoc-protected amino acids, N,N'-diisopropylcarbodiimide (DIC), and O-(7-azabenzotriazol-1-yl)-N,N,N',N'-tetramethyluronium hexafluorophosphate (HATU) were purchased from Chem-Impex International, Inc. RMPI-1640, FBS, L-glutamine, trypsin and EDTA solution, and 1× phosphate buffered saline (PBS) were purchased from Corning. Biotech CE dialysis tubing MWCO: 300kD, Ultrapure Low Melting Point Agarose, Nunc Lab-Tek Chambered Coverglass, sodium chloride (NaCl), hydrochloric acid (HCl), acetonitrile, trifluoroacetic acid (TFA), dichloromethane, dimethyl sulfoxide cell culture grade (DMSO), dimethylformamide (DMF), and formic acid LC/MS grade were purchased from Fisher. Calcium and magnesium free Dulbecco's phosphate-buffered saline (DPBS) was purchased from Gibco. Hoechst 33342 trihydrochloride trihydrate dye was purchased from Invitrogen. EmbryoMax 0.1% gelatin solution was purchased from Millipore. N,N-Diisopropylethylamine (DIEA) was purchased from Oakwood. Triton X-100 and potassium chloride (KCl) were purchased from Sigma. 2000 MWCO dialysis cassettes were purchased from Spectrum Labs. Anisole was purchased from Tokyo Chemical Industry. Tris and gentamycin were purchased from VWR. A549 and HeLa cells were obtained from the National Cancer Institute cell repository. Analytical LCMS solvents were composed

as follows: solvent A is 0.1% formic acid in water and solvent B is 9:1 acetonitrile and water with 0.1% formic acid. Preparative HPLC solvents consisted of solvent A (0.1% TFA in water) and solvent B (9:1 acetonitrile and water with 0.1% TFA).

2.2. Peptide synthesis and fluorescent labeling

Peptide synthesis was carried out via Fmoc-based solid-phase peptide synthesis with Oxyma/N,N'-Diisopropylcarbodiimide (DIC) activation on Rink Amide ProTide resin using a Liberty Blue Automated Microwave Peptide Synthesizer (CEM, Matthews, NC). Cleavage from the resin and side-chain deprotection was performed simultaneously using a trifluoroacetic acid:thioanisole:1,2-ethanedithiol:anisole (90:5:3:2) solution stirred under argon for 2 h. Cold diethyl ether was used to precipitate the crude peptide. After centrifugation at 5000 rpm for 5 min. to collect the solids, the diethyl ether was decanted and sample lyophilized overnight. Peptides were purified by reverse-phase HPLC (Shimadzu, Columbia, MD) equipped with a Phenomenex Semi-Prep Luna C18(2) column (Torrance, CA). A linear gradient of 0–50% solvent B over 50 min. was used to purify the Citropin peptide. A gradient of 0–20% solvent B over 10 min, followed by 20–44% solvent B over an additional 24 min, was used to purify Halictine. Purification of Lasioglossin was performed using a linear gradient of 0–14% solvent B over 7 min, followed by 14–45% solvent B over an additional 31 min. All peptides were lyophilized and pure product collected for verification by analytical LC-MS.

Fluorescently-labeled Lasioglossin was prepared by reacting the N-terminal amine of the peptide on resin with 5(6)-carboxyfluorescein (2 eq.), HATU (1.9 eq.), and N,N-diisopropylethylamine (DIEA, 6 eq.) overnight while shaking at room temperature. Normal cleavage and purification protocols were followed as described above. To purify the labeled Lasioglossin peptide, a linear gradient of 0–32% solvent B over 16 min, followed by 32–45% solvent B for an additional 13 min, was used. Analytical HPLC chromatograms and ESI (+) mass spectra for all pure peptides are shown in the [Supplementary Information, Figs. S1–S4](#).

2.3. Particle formulation and physicochemical characterization

Liposomes were formed using extrusion techniques as previously described [20]. To summarize, a 5 mM solution of 1:1 phosphatidylcholine (POPC):phosphatidylserine (POPS) lipids were combined in chloroform, followed by evaporation of the solvent under a stream of argon. The lipid film was then lyophilized overnight to dry completely, before rehydration with 2× concentrated liposome buffer (300 mM BTP, 100 mM NaF, and pH 7.4). The solution was then subjected to 8 freeze/thaw cycles in liquid nitrogen, with intermittent thawing performed using a 37 °C water bath. The solution was then extruded through an Avanti Mini Extruder (Alabaster, Alabama) with a 0.1 μm nuclepore polycarbonate membrane >11 times.

Formation of lipopeptisomes (LP) was performed by combining the 5 mM solution of liposomes in buffer with an equal volume of 2× concentrated solution of peptide in water, mixed and then incubated at 37 °C for 30 min to allow for interpolation. The LP solution was then dialyzed against water for 24 h using 300kD MWCO dialysis tubing, with frequent bath changes. Peptide loading was determined by measuring the absorbance of the purified particle solution at 220 nm using a Cary 60 UV-Vis spectrophotometer (Agilent Technologies, Santa Clara, CA), and concentration determined relative to a standard curve. Absorbance of blank liposomes was subtracted to normalize the signal. When necessary, the LP samples were concentrated in 0.5 mL Eppendorf tubes on a CentriVap Benchtop Vacuum Concentrator (Labconco, Kansas City,

MO) for one hour, or until the desired volume had been achieved, for subsequent *in vitro* experiments.

Size characterization of LP particles was completed by dynamic light scattering (DLS) using a Zetasizer Nano ZS (Malvern Instruments Ltd, Worcestershire, UK). In a typical experiment a 60 μL aliquot of the liposome solution in buffer was combined with an equal volume of peptide in water to achieve a final concentration of 0.01–1000 μM peptide. After incubating at 37 °C for 30 min, the solutions were then diluted 1:10 in particle characterization buffer (150 mM BTP, 50 mM NaF, pH 7.4) and placed into a clean polystyrene cuvette. DLS was performed at 37 °C with an equilibration time of 120 s, and average particle size determined from 6 replicates per sample. For LP stability studies, the particles were loaded with 100 μM of each peptide, or left unloaded as a 'blank' control. Particles were diluted 1:4 in storage buffer (20 mM Tris, 100 mM NaCl, pH 7.4) and stored at 37 °C, with DLS measurements performed at varied time points up to 110 days.

Transmission electron cryomicroscopy was performed on blank liposomes and LP particles by adsorbing an aqueous aliquot of the sample onto a quantafoil grid. The grid was then vitrified via plunge freezing using a Vitrobot (FEI, ThermoScientific), and imaged at 300 kV using a Krios cryo-EM (FEI, ThermoScientific).

2.4. Circular dichroism

Circular Dichroism (CD) was performed on a J-1500 Circular Dichroism Spectrometer (JASCO, Oklahoma City, OK) to determine the secondary structure of the peptides upon integration into LPs. Here, 200 μM of each peptide in characterization buffer was mixed with an equal volume of the liposomes (final lipid concentration of 2.5 mM). Wavelength spectra were measured from 180 to 260 nm at 37 °C in a 1 mm path length quartz cell. Mean residue molar ellipticity $[\theta]$, measured in (deg*cm²*dmol⁻¹), was calculated from the following expression: $\theta_{meas}/(10^3 * l * c * r)$ where θ_{meas} is measured ellipticity (mdeg), l is light path length (cm), c is molar concentration (mol/L), and r is number of amino acid residues.

2.5. Cell cytotoxicity assay

A549, HeLa and HUVEC cells were cultured using standard culturing conditions. For cell viability experiments, cells were seeded into a 96 well plate at 2×10^3 cells/well for A549 and HeLa, and 5×10^3 cells/well for HUVEC. Cells were allowed to adhere overnight before the media was aspirated and treatments of free peptides or LP formulations added in 10 fold dilutions to achieve a final concentration of 0.001–100 μM. Blank media and 20% DMSO were included as negative and positive controls, respectively. Treatments were incubated for 72 h before measurement of cell viability via MTT assay. Here, treatment solutions were aspirated and cells washed with PBS, before addition of 100 μL of 0.5 mg/mL thiazolyl blue tetrazolium bromide in media to each well and incubating for 2–3 h. Cells were subsequently lysed and the formazan byproduct solubilized by addition of 100 μL DMSO. Absorbance was read at 540 nm on with a microplate reader (Biotek, Winooski, VT). Percent viability was calculated with the following equation: $(\text{Absorbance}_{\text{treatment}} - \text{Absorbance}_{\text{negative control}}) / (\text{Absorbance}_{\text{positive control}} - \text{Absorbance}_{\text{negative control}}) \times 100\%$.

2.6. Confocal fluorescent microscopy

Visualization of LP fusion with cancer cells, and subcellular localization of lipid and peptide particle components, was performed via confocal microscopy. For these experiments, we prepared fluorescently labeled liposomes following the protocol above, with the exception that particles were composed of 49.5:50:0.5 POPC/POPS/PE_{rhodamine}. Loading of Lasioglossin into

the particles was performed at a final peptide concentration of 100 μM , where fluorescein-labeled peptide was doped in at a ratio of 10% with unlabeled Lasioglossin. A549 cells were seeded in 4-well coverglass chamber slides at 10,000 cells/well, and allowed to adhere overnight. Cells were treated with a final concentration of 20 μM labeled LPs in media for 24–72 h, or left untreated as controls. At each time point, the supernatant solution was removed, cells washed with cold PBS and fixed with 4% paraformaldehyde for 20 min at room temperature. Cell nuclei were then stained by the addition of 2 $\mu\text{g}/\text{mL}$ Hoechst in PBS and incubated in the dark for 20 min. Slides were imaged on an Olympus Fluoview 1000 Confocal Microscope (Olympus, Shinjuku, Tokyo, Japan) with a PlanApo 60 \times /1.4 oil objective lens using 405 nm, 488 nm, and 543 nm single photon lasers for DAPI, FITC, and rhodamine signals, respectively.

In separate experiments, we utilized giant unilamellar vesicles (GUVs) as a model to visualize ACP integration into lipid membranes. Formation of GUVs was performed as previously described [20]. In brief, a solution of 1 wt% low-melting agarose was added to a 4-well chambered slide until it just covered the glass surface. The chambered coverglass was then dried on a 45 $^{\circ}\text{C}$ hotplate for 1 h until the agarose became translucent. After preparing a 3.75 mg/mL lipid solution of POPC, POPS, PE, and PE_{rhodamine} in chloroform, 4 μL was added to each chamber and a metal spatula gently dragged across the surface to evenly distribute the solution. The chambered coverglass was then lyophilized overnight to dry. Swelling of the GUVs occurred by adding 500 μL of 150 mM KCl solution to each well. After 15 min to allow for GUV fusion, 10 μL of a 500 μM fluorescein-labeled Lasioglossin solution was added to each chamber to initiate treatment. Slides were mounted onto an Olympus Fluoview 1000 confocal microscope and imaged using a PlanApo 60 \times /1.4 oil objective lens. 488 nm and 543 nm single photon lasers were used to visualize fluorescein and rhodamine fluorescence, respectively. Relative fluorescence (RF) was calculated using Fiji – ImageJ software by measuring the intensity of the fluorescein signal within a region of the GUV membrane and subtracting the background fluorescence from the surrounding bulk solution for each time point.

2.7. Hemolysis

Hemolysis studies began by obtaining fresh human blood samples and isolating red blood cells via centrifugation at 3460 rpm for 10 min. at 4 $^{\circ}\text{C}$. The plasma and buffy coat layers were removed and hRBCs washed three times in un-supplemented RPMI. A 0.25% v/v solution of the washed hRBCs was prepared in RPMI, and a 75 μL aliquot added per well to a 96 well plate. Equal volume of free peptide or LP solutions were added to the RBC sample and gently mixed via pipette to achieve a final equivalent peptide concentration of 10–100 μM . Blank RPMI or 1% Triton-X100 were used as negative and positive controls, respectively. Plates were then incubated at 37 $^{\circ}\text{C}$ for 24 h, before centrifugation at 4000 rpm for 10 min. at 4 $^{\circ}\text{C}$ to pellet intact hRBCs. 100 μL of the hRBC supernatant was added to a clean 96 well plate and absorbance of released hemoglobin measured at 415 nm in a microplate reader (Biotek, Winooski, VT). The following equation was used to calculate percent hemolysis: $(\text{Absorbance}_{\text{treated}} - \text{Absorbance}_{\text{negative control}}) / (\text{Absorbance}_{\text{positive control}} - \text{Absorbance}_{\text{negative control}}) \times 100\%$.

2.8. Statistical methods

Dynamic light scattering and absorbance data is the average of three replicates \pm standard deviation. Each UV–Vis and CD spectra, as well as fluorescent confocal and TEM micrographs, shown are representative of three individual experiments. CD data is with a variance in ellipticity of 0.2 millidegrees at each wavelength.

Relative fluorescence data calculated from fluorescent confocal images represents the average of 10 independent measurements \pm standard deviation. Cytotoxicity data is represented as an average of three independent experiments \pm standard deviation. GraphPad Prism 5 software was used to fit cytotoxicity curves and calculate IC_{50} values employing a log(inhibitor) vs. normalized response non-linear regression model. For hemolysis experiments each treatment condition was performed in triplicate and average \pm standard deviation calculated.

3. Results and discussion

3.1. LP design, formulation and characterization

To design LPs we selected three ACPs reported to possess potent oncolytic activity ($\text{IC}_{50} < 15 \mu\text{M}$), namely A4K14-Citropin 1.1, Halictine-2/11 and Lasioglossin-III (Table 1). For simplicity, the peptides will be hereafter referred to as Citropin, Halictine and Lasioglossin. These sequences, which were discovered in amphibian secretions and bee venoms, were initially characterized as broad spectrum antimicrobials before later discovery of their anti-cancer properties [21–23]. In the case of Citropin and Halictine, the sequences have undergone further optimization to yield engineered analogues (e.g. A4K14-citropin 1.1, Halictine-2/11) with enhanced oncolytic potency [21,22]. In both prokaryotic and eukaryotic cells, these peptides elicit their toxic action primarily by binding to the negatively charged cell membrane and partitioning into the lipid bilayer [21–24]. Subsequent folding into amphipathic α -helical conformations and self-assembly of the peptides leads to cell death via the formation of lytic pores, or through the solubilization of membrane constituents in a detergent-like fashion [1,3,16,23].

Despite their significant therapeutic potential, all three of these sequences suffer from low therapeutic indices due to significant off-target hemolysis. Thus, these peptides serve as ideal models to test the potential for LPs to enhance the therapeutic utility of previously toxic ACPs. Conveniently, the selected peptides also possess varied amino acid composition, sequence length and formal charge (see Table 1), and therefore can be used to assess the potential of LPs to tolerate loading of peptide cargoes with diverse physicochemical properties.

To prepare LP particles, we incubated ACPs at various concentrations with ~ 150 nm liposomes, leading to direct interpolation of the peptides within the lipid nanoparticle bilayer. Importantly, the liposomal carrier is formed using a 1:1 M ratio of phosphatidylcholine (PC) and phosphatidylserine (PS). This formulation mimics the aberrant lipid composition of the cancer cell membrane [25], which is characterized by increased presentation of anionic PS lipids at the outer leaflet [4,6]. We, and others, have shown that this high density of PS imparts an electronegative surface potential that triggers the selective binding and folding of cationic ACPs into their bioactive lytic states [12,14,25–27].

Using dynamic light scattering (DLS), we measured the influence of increasing amounts of loaded peptide on LP stability, expressed as a peptide:lipid ratio. Fig. 2A shows that LPs remain stable up to ratios of 0.04:1–0.2:1, dependent on the sequence employed. Representative particle size distribution plots for blank liposomes and the three LP formulations can be found in supplementary Fig. S5. Increasing the ACP concentration beyond this failure threshold destabilized the lipid bilayer and led to particle rupture, as indicated by the complete loss of DLS signal. This suggests that the failed particles disassociate into ultrafine fragments not detectable by the light scattering instrument (< 5 nm). Importantly, given the propensity of these ACPs to lyse lipid membranes, the ability of LPs to support relatively high peptide:lipid ratios is

Table 1
Sequence, physicochemical properties and reference for selected ACPs utilized to prepare LPs.

Peptide	Sequence ^a	# AA	Formal charge ^b	Ref.
A4K14-citropin 1.1	GLFAVIKQVASVIKGL-NH ₂	16	+4	12
Halictine-2/11	GKWLSLLKHILK-NH ₂	12	+5	13
Lasioglossin-III	VNWKILGKIIVVK-NH ₂	15	+6	13

^a All peptides are prepared with amidated C-terminus.

^b Formal charge includes N-terminal amine. Histidine considered partially protonated for purposes of formal charge calculation.

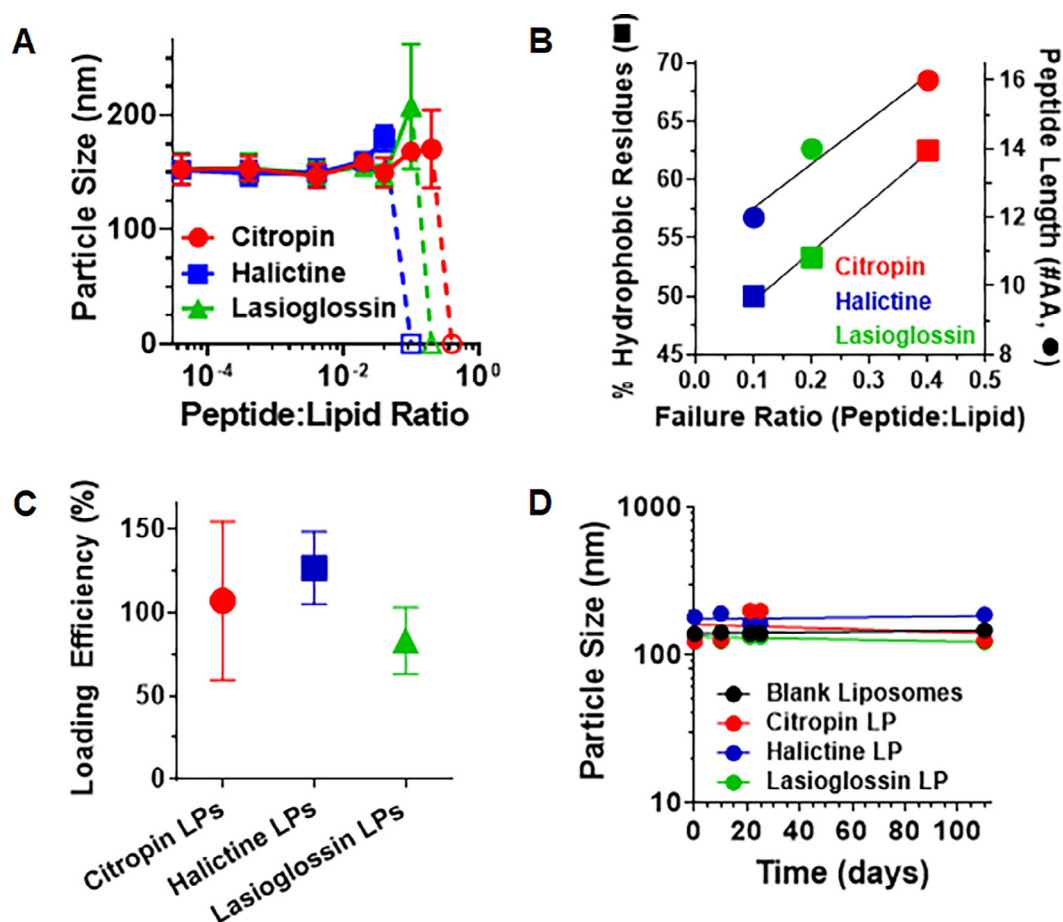


Fig. 2. Preparation and physicochemical characterization of LPs. (A) Change in LP particle size as a function of increasing peptide:lipid ratio. Dashed line and open symbols indicate particle failure, as defined by the loss of DLS signal. (B) Change in the LP peptide:lipid failure ratio as a function of ACP hydrophobicity (% hydrophobic residues in the sequence; ■) or peptide length (number of amino acids; ●). (C) Percentage loading efficiency of each ACP into the final LP formulation. (D) Stability of LP particles, or the blank liposomal carrier, during long term-storage in buffer at room temperature. Particle stability was measured via DLS.

surprising. For example, we found that Citropin formulations can be loaded with up to ~30 wt% of peptide, indicating that under these conditions integrated ACPs make up nearly a third of the LP particle by weight.

To better understand what drives this proficient loading of ACPs into the lipid carrier, we examined the influence of peptide physicochemical properties on LP stability. This was done by plotting the LP failure ratio, or the peptide:lipid threshold at which particle integrity is lost, against various sequence parameters, including peptide length, percentage of hydrophobic or basic residues, and formal charge. Results in Fig. 2B show a linear relationship between LP failure ratio and both peptide length and sequence hydrophobicity. No significant correlation with peptide formal charge, as well as percentage of basic residues in the ACP sequence, was observed (Supplementary Fig. S6). Taken together, this suggests that maximal loading of ACPs into the particle lamella is

largely dependent on the lipophilic nature of the peptide, as well as the number of amino acids in its sequence. The latter likely results from the ability for longer helical peptides (>13 residues) to more stably insert into fluid lipid membranes and span the bilayer thickness (~44 Å) as a transmembrane helix [28,29].

From these loading experiments we selected a peptide:lipid ratio of 0.02:1, representing 100 μM equivalent peptide, to prepare LPs for further studies as this produced stable formulations for all three ACPs tested. Cryo-TEM imaging of LPs, or the unloaded liposomal carrier as a control, showed no discernable change in particle morphology following integration of ACPs into the bilayer (Supplementary Fig. S7). To assess loading efficiency, we prepared LPs with each peptide, purified the particles via dialysis to remove unincorporated ACPs, and performed UV–Vis spectroscopy to measure the concentration of incorporated peptide. In the case of Halictine and Lasioglossin, their efficient integration into the carrier

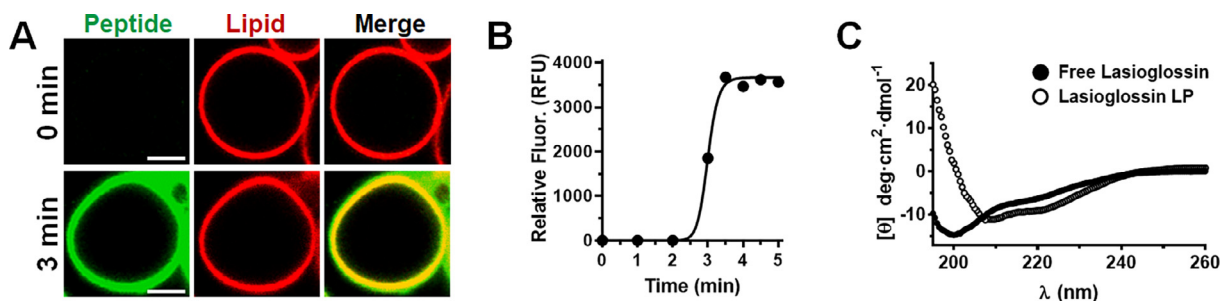


Fig. 3. ACP localization and folding within the LP carrier. (A) Fluorescent confocal microscopy images of giant unilamellar vesicles (GUVs) showing the integration of fluorescein-labeled Lasioglossin (green) before (0 min) and 3 min. after addition of the peptide (scale bar = 5 μm). GUVs were prepared at a 30:40:30 ratio of PS:PC:PE lipids, with 0.5 mol% of rhodamine-labeled PE included to aid in visualization (red). Merged image shows co-localization of peptide and lipid fluorescent signals. (B) Quantification of Lasioglossin fluorescence (in relative fluorescence units, RFU) at the GUV membrane as a function of time. (C) Circular dichroism spectrum demonstrating that Lasioglossin remains unfolded in physiologic buffer (\bullet), but adopts an α -helical conformation when integrated into the negatively-charged lipid carrier to form LPs (\circ). CD spectrum of Citropin and Halictine LPs shown in Supplementary Fig. S9.

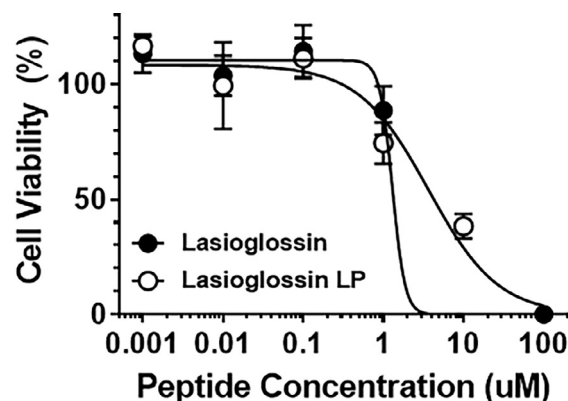
was evidenced by the emergence of a broad peak at 280 nm, reflecting the characteristic absorption maxima of tryptophan residues in the loaded ACP (Supplementary Fig. S8). Calculating peptide concentration shows that Citropin and Halictine achieve quantitative loading into LPs of $\sim 100\%$, while Lasioglossin shows an average efficiency of 83% (Fig. 2C). Finally, all three LP formulations were found to be stable when stored in buffer for over 100 days (Fig. 2D).

Next, utilizing giant unilamellar vesicles as a model membrane, we performed fluorescent confocal microscopy to study the localization of ACPs when loaded into the lipid carrier. This is important as effective delivery of ACPs into the cancer cell membrane during LP fusion requires incorporated peptides to be resident within the lipid corona, rather than adsorbed to the particle surface or dispersed within the solvent core. Images in Fig. 3A show that fluorescently-labeled Lasioglossin rapidly integrates into the vesicular lipid bilayer and spans the unilamellar membrane, reaching maximum incorporation within 3.5 min of addition (Fig. 3B). Circular dichroism spectroscopy demonstrates that all three ACPs remain disordered in physiologic buffer before particle binding, but display a strong α -helical signal characterized by minima in mean residue ellipticity at 208 nm and 222 nm upon incorporation within the negatively-charged liposomal carrier (Fig. 3C, Supplementary Fig. S9). Taken together, these results confirm that ACPs rapidly integrate across the lipid bilayer to prepare LPs, and in doing so pre-fold into α -helical conformations that are essential for their cytotoxic activity [23,30,31].

3.2. Membrane fusion and anticancer activity of LPs

The preferential anticancer activity of free ACPs or peptide-loaded LP formulations was evaluated via the MTT assay following a 72 h incubation with A549 lung carcinoma or HeLa cervical cancer cells, as well as non-cancerous HUVECs (human umbilical vein endothelial cells) as a control (Fig. 4). These studies test the ability of LPs to selectively deliver ACP cargo to cancer cells without influencing its lytic activity once integrated into the membrane. If the lipid carrier is inert and able to efficiently deliver the payload into tumor cells, we would expect a similar activity of ACP-loaded LPs with the corresponding free peptide. Gratifyingly, treatment of both A549 and HeLa cancer cell lines with all three LP formulations resulted in potent cytotoxic activity ($\text{IC}_{50} = 1.0\text{--}5.2\ \mu\text{M}$), which is on the order of the free peptides ($\text{IC}_{50} = 1.3\text{--}5.1\ \mu\text{M}$).

Conversely, we observed a notable reduction in the off-target toxicity of ACPs towards healthy HUVEC controls when peptides are loaded into the LP carrier. In fact, we were unable to calculate exact IC_{50} values for the particles as we did not observe any signif-



Treatment	IC_{50} (μM)		
	A549	HeLa	HUVEC
Citropin	4.8 ± 1.8	2.2 ± 0.3	6.4 ± 2.2
Citropin LP	5.2 ± 1.7	3.3 ± 0.5	>50
Halictine	5.1 ± 1.6	2.0 ± 0.4	21.6 ± 2.4
Halictine LP	5.2 ± 3.4	2.3 ± 0.2	>50
Lasioglossin	1.3 ± 2.5	1.3 ± 1.2	29.6 ± 3.0
Lasioglossin LP	1.0 ± 1.3	3.8 ± 0.9	>50

Fig. 4. (Top) Representative cytotoxicity profile of free Lasioglossin and the corresponding LP formulation against HeLa (cervical carcinoma) cells. (Bottom) Tabulated IC_{50} values \pm standard deviation for each ACP and its corresponding LP particle formulation after a 72 h incubation with A549 (lung carcinoma) and HeLa cancer cell lines, or non-cancerous HUVECs (human umbilical vein endothelial cell) as a control.

icant loss of HUVEC viability, even at the highest peptide loading concentration tested (50 μM). In the case of Citropin, toxicity of this peptide towards HUVECs is reduced by nearly an order of magnitude when delivered by LPs. This improvement in ACP specificity when formulated into an LP particle may be due to a reduced potential for fusion of the lipidic carrier with the healthy mammalian cell membrane, relative to tumor cells. The outer leaflet of non-cancerous cells is characterized by high PC content [17,18], which is a lipid whose headgroup strongly binds water to establish a lipid-water interface that prevents contact-mediated fusion with nearby bilayers [32]. Further, the surfaces

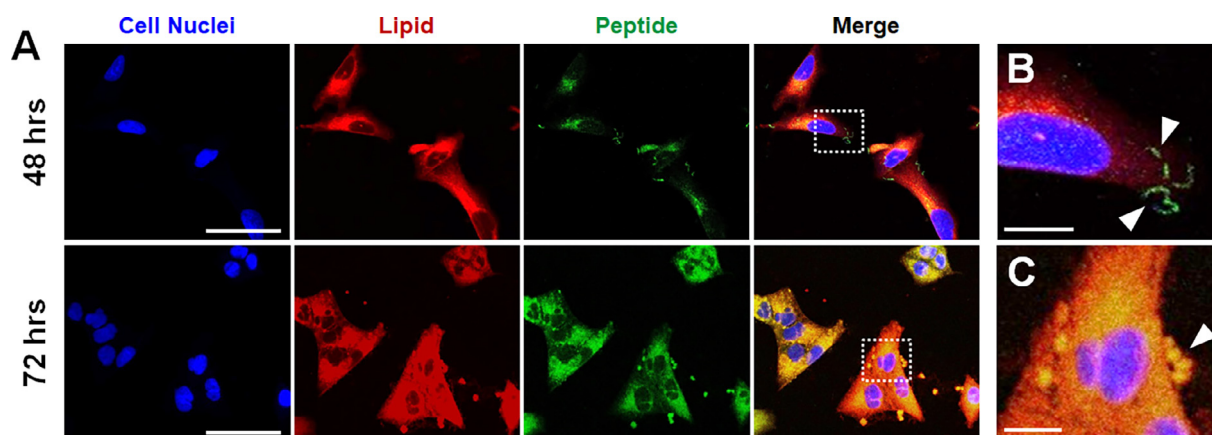


Fig. 5. LP integration into cancer cells and subcellular tracking of delivered lipids (red) and ACPs (green). (A) Fluorescent confocal microscopy images of A549 lung carcinoma cells treated for 48 or 72 h with Lasioglossin LPs (scale bar = 50 μm). Magnification of dotted regions in the 48 and 72 h merged images are shown in panels B and C, respectively. (B) Assembly of LP-delivered Lasioglossin into fibrillary structures (white arrow) at the cancer cell surface (scale bar = 10 μm). (C) Nuclear fragmentation and membrane blebbing (white arrow) of A549 cells following a 72 h incubation with labeled Lasioglossin LPs (scale bar = 10 μm).

of healthy mammalian cells are scarce of PS lipids [17,18], which are abundant on the outer leaflet of cancer cells due to the aberrant function of enzymes responsible for maintaining proper lipid asymmetry in malignant phenotypes [4–6]. Relevant to the function of LP particles, PS is a key mediator of membrane fusion due to its ability to bind divalent Ca^{2+} cations that are responsible for removing water from the lipid interface [32,33]. Taken together, these results strongly support the ability of LPs to preferentially fuse with tumor cells and successfully integrate the lytic ACP payload into the membrane, while circumventing off-target toxicity of the peptide cargo towards healthy tissues.

To further test this assertion, as well as directly visualize LP integration and ACP assembly within tumor cell membranes, we performed confocal microscopy employing dual-labeled LP formulations. Here, the liposomal carrier and loaded ACP were independently labeled with rhodamine and fluorescein fluorophores, respectively, to visualize subcellular localization of each component upon LP-membrane fusion (Fig. 5). Fluorescent microscopy images collected at 24 and 48 h (Supplementary Fig. S10 and Fig. 5A, respectively) show that the lipid carrier (red) is rapidly integrated into treated cancer cells and shows diffuse localization across the membrane and cytoplasmic compartments. Corresponding differential interference contrast (DIC) images of LP-incubated cells and untreated controls can be found in Supplementary Fig. S11. This extensive particle uptake likely results from the upregulation of pathways responsible for scavenging and internalizing exogenous lipids in cancer cells, a necessary requirement to meet the high metabolic demands of these rapidly proliferating cells [34,35]. Internalized lipids are subsequently processed through catabolic fatty acid oxidation pathways and used to form new membrane constituents and signaling molecules, as well as to post-translationally modify proteins. This may explain the broad dissemination of the lipid signal observed following the assimilation of LPs into treated cancer cells at all tested time points.

Interestingly, delivered ACPs were localized predominantly to the cancer cell surface as assemblies of micron-sized proto-fibrils at 24 and 48 h of incubation (Supplementary Fig. S10 and Fig. 5B). To our knowledge, this is the first time higher ordered ACP structures have been resolved by confocal microscopy following peptide self-assembly within cancer cell membranes. We also found that a portion of delivered ACPs are transported intracellularly, appearing as diffuse fluorescence within the cytoplasm of treated cells. This is particularly evident at 72 h of incubation (Fig. 5A, lower panels). Together this suggests that at early time

points much of the delivered ACP cargo self-associates in the cancer cell membrane to form higher ordered lytic structures, followed later by shuttling of the peptides to endosomal and cytoplasmic intracellular compartments during membrane turnover. Based on these observations, we cannot rule out the fact that intracellularly delivered ACPs may be able to permeabilize mitochondrial membranes inside cells and induce apoptosis. This is supported by the representative image shown in Fig. 5C, which indicates that at 72 h LP-treated cancer cells begin to display fragmented nuclei and undergo membrane destabilization, as indicated by lipid blebbing at the cell surface (see white arrows in Fig. 5C). Hence, LPs may kill cancer cells through combinatorial mechanisms that include both physical membrane lysis and induction of apoptotic pathways.

3.3. Hemolytic activity of LP particles

We next studied the cytotoxic selectivity of LPs with respect to their ability to lyse tumor cells versus healthy human erythrocytes. Like all mammalian cells, the surface of red blood cells (RBCs) are composed largely of cholesterol and various phospholipids that are asymmetrically separated across an inner and outer leaflet [19]. Previous studies have shown that the presence of negatively charged lipids, such as phosphatidylethanolamine, on the outer leaflet of red blood cells potentiates the off-target binding of ACPs to their surfaces and leads to hemolysis, with lytic potency generally associated with peptide hydrophobicity and helicity [36]. To assess potential reduction in ACP hemolytic toxicity when loaded into the LP carrier, we first measured the integrity of RBCs following a 24 h incubation with each ACP at a representative low (10 μM) and high (100 μM) peptide concentration (Fig. 6). Not surprisingly, under these conditions we observed moderate (18–36%) hemolysis at the low ACP concentration tested, and complete destruction of RBCs at 100 μM of peptide (Fig. 6, left). Remarkably, the toxicity of these sequences was reduced by nearly two orders of magnitude when incorporated within LPs. For example, all three LP formulations showed $\leq 8\%$ hemolysis at the highest tested concentration of loaded ACP (100 μM). In fact, under these stringent incubation conditions both Citropin and Halictine LP formulations elicited $< 5\%$ total hemolysis, which is the threshold at which materials are considered non-hemolytic by ASTM guidelines (see protocol ASTM-F756).

From this data we can calculate an approximate therapeutic index (the ratio of therapeutic vs. toxic dose) for each LP formula-

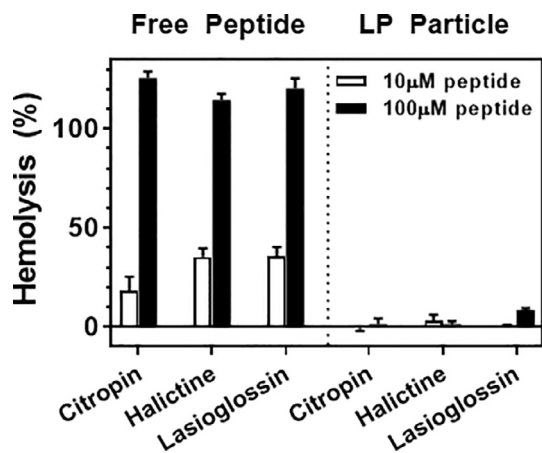


Fig. 6. Percentage hemolysis of human RBCs following a 24 h incubation with (Left) free Citropin, Halictine and Lasioglossin ACPs, or the (Right) corresponding LP particle formulation. Hemolytic activity for each treatment condition tested is shown at a low (10 μM, white bar) or high (100 μM, black bar) concentration of equivalent peptide. Data is normalized to untreated hRBCs, and percent hemolysis calculated relative to positive controls lysed with Triton-X.

tion by dividing the hemolytic threshold (~100 μM) by the average IC_{50} value for each particle towards cancer cells (Fig. 4). This analysis reveals that LP particles possess a therapeutic index of 24, 27 and 42 for Citropin, Halictine and Lasioglossin formulations, respectively. Gratifyingly, all three of these LP formulations are characterized by therapeutic indices amenable to clinical application, being well above that of most chemotherapeutic agents [37].

This significant reduction in the hemolytic potential of ACPs when incorporated within the LP carrier may be a result of the unique composition of the RBC surface. First, erythrocytes lack the lipid scavenging receptors displayed on other mammalian cell types, and which are particularly abundant on cancer cells [34,35,38]. This suggests that LPs may be poorly recruited to the surfaces of RBCs and thus limited in their ability to fuse to the membrane and integrate the lytic ACP payload. Second, the vast majority of PS content in the healthy RBC bilayer is confined to the inner leaflet in order to prevent premature clearance by immune cells [19,39]. Relevant to the activity of our LP particles, PS is a key mediator of membrane fusion due to its ability to bind divalent Ca^{2+} cations that are responsible for removing water from the lipid interface [32,33]. This ultimately allows more intimate contact between dehydrated bilayers and the nucleation of lamellar defects that are a pre-requisite for initiation of membrane fusion. In addition to this distinct lack of PS, the outer monolayer of RBCs is rich with PC lipids, which possess a headgroup that tightly binds to water and as a result potentially inhibits interbilayer fusion [19,32]. Taken together, this suggests that the compositional mismatch of lipids in our particles and the erythrocyte membrane may ultimately hinder LP fusion with RBCs, and instead shift their preferential interaction towards the PS-rich surface of cancer cells [4–6].

4. Conclusions

In this work we report the design and efficacy of fusolytic nanoscale particles prepared via the interpolation of membrane-active helical peptides into liposomal lamella. The resulting particles, referred to as lipopeptisomes, can be efficiently loaded with oncolytic ACPs and remain stable during long term storage. We show that incorporation of ACPs within LP particles did not disrupt or diminish their lytic behavior, leading to proficient assimilation of the peptides into cancer cells membranes and potent cytotoxicity

profiles. Interestingly, when taken within the broader context of the biophysical mechanisms that mediate interbilayer fusion, our work provides new insights into the potential to target nanoparticles to specific cell types via compositional matching of particle-cell lipid constituents.

With respect to the clinical utility of ACPs, this new delivery strategy is able to impart a significant improvement in the anti-cancer specificity of oncolytic peptides by reducing their off-target hemolytic potential and toxicity towards healthy, non-cancerous tissues. As a result, previously toxic ACPs are transformed into potential drug candidates that can be considered ‘non-hemolytic’ by ASTM guidelines and which possess clinically relevant therapeutic indices. In fact, LPs display therapeutic windows well above that of many clinically employed chemotherapeutics [40]. These nanomaterials even exceed the toxicity profile of some antibiotics, such as vancomycin (index ~10) [41], which are often considered the paragon class of therapeutics with which to benchmark biocompatibility.

It is worth noting that in our studies the tolerance of LPs was established based on their *in vitro* profile, and thus we cannot rule out the potential for secondary effects *in vivo*. However, the fact that hemolytic toxicity remains a key barrier to the clinical translation of many membrane-active peptides [15], and combined with the low toxicity and immunogenicity profiles of lipid nanoparticles [42], suggests that LPs represent a biocompatible delivery platform with significant potential to advance new oncolytic strategies in the clinic. Thus, we present a novel delivery modality poised to improve the utility of ACPs, open up new combinatorial approaches in oncology, and may add to our arsenal of strategies to combat the emergence of therapeutic resistance in precision medicine.

Acknowledgements

We thank the laboratory of Dr. Joel Schneider at the National Cancer Institute for providing cancer cell lines. We also recognize and thank the Penn State Microscopy and Cytometry Facility – University Park, PA for assistance with confocal microscopy and cryo-TEM sample prep, imaging and analysis. We also acknowledge the Penn State X-Ray Crystallography Facility – University Park, PA and Penn State Materials Characterization Laboratory – University Park, PA for use of the CD spectrophotometer and dynamic light scattering instrumentation, respectively. This work is supported by laboratory startup funds provided to S.H. Medina by the Pennsylvania State University. M.R. Aronson was supported by funds from the Penn State Schreyer Honors College Independent Research Grant and the Penn State Student Engagement Network Grant. All authors declare no conflict of interest.

Appendix A. Supplementary data

Supplementary data to this article can be found online at <https://doi.org/10.1016/j.actbio.2018.09.025>.

References

- [1] C. Leuschner, W. Hansel, Membrane disrupting lytic peptides for cancer treatments, *Curr. Pharma. Des.* 10 (19) (2004) 2299–2310.
- [2] F. Schweizer, Cationic amphiphilic peptides with cancer-selective toxicity, *Eur. J. Pharmacol.* 625 (1) (2009) 190–194.
- [3] D. Gaspar, A.S. Veiga, M.A. Castanho, From antimicrobial to anticancer peptides. A review, *Front. Microbiol.* 4 (2013) 294.
- [4] K. Balasubramanian, A.J. Schroit, Aminophospholipid asymmetry: a matter of life and death, *Annu. Rev. Physiol.* 65 (1) (2003) 701–734.
- [5] R.A. Chaurio, C. Janko, L.E. Muñoz, B. Frey, M. Herrmann, U.S. Gaip, Phospholipids: key players in apoptosis and immune regulation, *Molecules* 14 (12) (2009) 4892–4914.

- [6] R. Zwaal, P. Comfurius, E. Bevers, Surface exposure of phosphatidylserine in pathological cells, *Cell. Mol. Life Sci.* 62 (9) (2005) 971–988.
- [7] W.-H. Yoon, H.-D. Park, K. Lim, B.-D. Hwang, Effect of O-glycosylated mucin on invasion and metastasis of HM7 human colon cancer cells, *Biochem. Biophys. Res. Commun.* 222 (3) (1996) 694–699.
- [8] M.D. Burdick, A. Harris, C.J. Reid, T. Iwamura, M.A. Hollingsworth, Oligosaccharides expressed on MUC1 produced by pancreatic and colon tumor cell lines, *J. Biol. Chem.* 272 (39) (1997) 24198–24202.
- [9] C.A. Reis, H. Osorio, L. Silva, C. Gomes, L. David, Alterations in glycosylation as biomarkers for cancer detection, *J. Clin. Path.* 63 (4) (2010) 322–329.
- [10] N. Papo, Y. Shai, Host defense peptides as new weapons in cancer treatment, *Cell. Mol. Life Sci.* 62 (7–8) (2005) 784–790.
- [11] A.L. Hilchie, C.D. Doucette, D.M. Pinto, A. Patrzykat, S. Douglas, D.W. Hoskin, Pleurocidin-family cationic antimicrobial peptides are cytolytic for breast carcinoma cells and prevent growth of tumor xenografts, *Breast Cancer Res.* 13 (5) (2011) R102.
- [12] S.H. Medina, J.P. Schneider, Cancer cell surface induced peptide folding allows intracellular translocation of drug, *J. Control. Release* 209 (2015) 317–326.
- [13] H. Zhao, X. Qin, D. Yang, Y. Jiang, W. Zheng, D. Wang, Y. Tian, Q. Liu, N. Xu, Z. Li, The development of activatable lytic peptides for targeting triple negative breast cancer, *Cell Death Discovery* 3 (2017) 17037.
- [14] K. Ishikawa, S.H. Medina, J.P. Schneider, A.J. Klar, Glycan alteration imparts cellular resistance to a membrane-lytic anticancer peptide, *Cell Chem. Biol.* 24 (2) (2017) 149–158.
- [15] S. Riedl, D. Zweyck, K. Lohner, Membrane-active host defense peptides—challenges and perspectives for the development of novel anticancer drugs, *Chem. Phys. Lipids* 164 (8) (2011) 766–781.
- [16] M.R. Felicio, O.N. Silva, S. Gonçalves, N.C. Santos, O.L. Franco, Peptides with dual antimicrobial and anticancer activities, *Front. Chem.* 5 (2017) 5.
- [17] G. van Meer, D.R. Voelker, G.W. Feigenson, Membrane lipids: where they are and how they behave, *Nat. Rev. Mol. Cell Biol.* 9 (2) (2008) 112–124.
- [18] H.I. Ingólfsson, M.N. Melo, F.J. Van Eerden, C. Arnarez, C.A. Lopez, T.A. Wassenaar, X. Periole, A.H. De Vries, D.P. Tieleman, S.J. Marrink, Lipid organization of the plasma membrane, *J. Am. Chem. Soc.* 136 (41) (2014) 14554–14559.
- [19] N. Mohandas, P.G. Gallagher, Red cell membrane: past, present, and future, *Blood* 112 (10) (2008) 3939–3948.
- [20] S.H. Medina, S.E. Miller, A.I. Keim, A.P. Gorka, M.J. Schnermann, J.P. Schneider, An intrinsically disordered peptide facilitates non-endosomal cell entry, *Angew. Chem. Int. Ed.* 55 (10) (2016) 3369–3372.
- [21] J. Doyle, C.S. Brinkworth, K.L. Wegener, J.A. Carver, L.E. Llewellyn, I.N. Olver, J.H. Bowie, P.A. Wabnitz, M.J. Tyler, nNOS inhibition, antimicrobial and anticancer activity of the amphibian skin peptide, citropin 1.1 and synthetic modifications, *Eur. J. Biochem.* 270 (6) (2003) 1141–1153.
- [22] J. Slaninová, V. Mlsová, H. Kroupová, L. Alán, T. Tümová, L. Monincová, L. Borovičková, V. Fučík, V. Čeřovský, Toxicity study of antimicrobial peptides from wild bee venom and their analogs toward mammalian normal and cancer cells, *Peptides* 33 (1) (2012) 18–26.
- [23] D.I. Fernandez, J.D. Gehman, F. Separovic, Membrane interactions of antimicrobial peptides from Australian frogs, *Biochim. Biophys. Acta* 1788 (8) (2009) 1630–1638.
- [24] Č. Václav, B. Miloš, H. Oldřich, C. Josef, V. Zdeněk, S. Jiřina, B. Lenka, F. Vladimír, B. Lucie, V. Ivan, S. Jakub, Lasioglossins: three novel antimicrobial peptides from the venom of the eusocial bee *lasioglossum laticeps* (Hymenoptera: Halictidae), *ChemBioChem* 10 (12) (2009) 2089–2099.
- [25] C. Sinthuvanich, A.S. Veiga, K. Gupta, D. Gaspar, R. Blumenthal, J.P. Schneider, Anticancer β -hairpin peptides: membrane-induced folding triggers activity, *J. Am. Chem. Soc.* 134 (14) (2012) 6210–6217.
- [26] D. Gaspar, A.S. Veiga, C. Sinthuvanich, J.P. Schneider, M.A.R.B. Castanho, Anticancer peptide SVS-1: efficacy precedes membrane neutralization, *Biochemistry* 51 (32) (2012) 6263–6265.
- [27] C. Wang, Y.-W. Chen, L. Zhang, X.-G. Gong, Y. Zhou, D.-J. Shang, Melanoma cell surface-expressed phosphatidylserine as a therapeutic target for cationic anticancer peptide, temporin-1CEa, *J. Drug Target* 24 (6) (2016) 548–556.
- [28] C. Baeza-Delgado, G. von Heijne, M.A. Marti-Renom, I. Mingarro, Biological insertion of computationally designed short transmembrane segments, *Sci. Rep.* 6 (2016) 23397.
- [29] N. Kučerka, M.A. Kiselev, P. Balgavý, Determination of bilayer thickness and lipid surface area in unilamellar dimyristoylphosphatidylcholine vesicles from small-angle neutron scattering curves: a comparison of evaluation methods, *Eur. Biophys. J.* 33 (4) (2004) 328–334.
- [30] L. Monincová, M. Buděšínský, J. Slaninová, O. Hovorka, J. Cvačka, Z. Voburka, V. Fučík, L. Borovičková, L. Bednářová, J. Straka, V. Čeřovský, Novel antimicrobial peptides from the venom of the eusocial bee *Halictus sexincinctus* (Hymenoptera: Halictidae) and their analogs, *Amino Acids* 39 (3) (2010) 763–775.
- [31] V. Čeřovský, M. Buděšínský, O. Hovorka, J. Cvačka, Z. Voburka, J. Slaninová, L. Borovičková, V. Fučík, L. Bednářová, I. Votruba, Lasioglossins: three novel antimicrobial peptides from the venom of the eusocial bee *Lasioglossum laticeps* (Hymenoptera: Halictidae), *ChemBioChem* 10 (12) (2009) 2089–2099.
- [32] N. Düzgünes, J. Wilschut, R. Fraley, D. Papahadjopoulos, Studies on the mechanism of membrane fusion. Role of head-group composition in calcium- and magnesium-induced fusion of mixed phospholipid vesicles, *Biochim. Biophys. Acta* 642 (1) (1981) 182–195.
- [33] J.C. Hay, Calcium: a fundamental regulator of intracellular membrane fusion?, *EMBO Rep* 8 (3) (2007) 236–240.
- [34] E. Currie, A. Schulze, R. Zechner, T.C. Walther, R.V. Farese, Cellular fatty acid metabolism and cancer, *Cell Metab.* 18 (2) (2013) 153–161.
- [35] S. Beloribi-Djefafliia, S. Vasseur, F. Guillaumond, Lipid metabolic reprogramming in cancer cells, *Oncogenesis* 5 (2016) e189.
- [36] Y.-B. Huang, L.-Y. He, H.-Y. Jiang, Y.-X. Chen, Role of helicity on the anticancer mechanism of action of cationic-helical peptides, *Int. J. Mol. Sci.* 13 (6) (2012) 6849–6862.
- [37] L. Alnaim, Therapeutic drug monitoring of cancer chemotherapy, *J. Oncol. Pharm. Practice* 13 (4) (2007) 207–221.
- [38] T.L. Steck, The organization of proteins in the human red blood cell membrane: a review, *J. Cell Biol.* 62 (1) (1974) 1–19.
- [39] R.F. Zwaal, A.J. Schroit, Pathophysiological implications of membrane phospholipid asymmetry in blood cells, *Blood* 89 (4) (1997) 1121–1132.
- [40] A. Paci, G. Veal, C. Bardin, D. Levêque, N. Widmer, J. Beijnen, A. Astier, E. Chatelut, Review of therapeutic drug monitoring of anticancer drugs part 1 – Cytotoxics, *Eur. J. Cancer* 50 (12) (2014) 2010–2019.
- [41] E.J. Begg, M.L. Barclay, C.J.M. Kirkpatrick, The therapeutic monitoring of antimicrobial agents, *Br. J. Clin. Pharmacol.* 47 (1) (1999) 23–30.
- [42] T.M. Allen, P.R. Cullis, Liposomal drug delivery systems: from concept to clinical applications, *Adv. Drug Delivery Rev.* 65 (1) (2013) 36–48.